Mergos, P.E. & Kappos, A. J. (2013). A combined local damage index for seismic assessment of existing RC structures. Earthquake Engineering and Structural Dynamics, 42(6), pp. 833-852. doi: 10.1002/eqe.2247

City Research Online

Original citation: Mergos, P.E. & Kappos, A. J. (2013). A combined local damage index for seismic assessment of existing RC structures. Earthquake Engineering and Structural Dynamics, 42(6), pp. 833-852. doi: 10.1002/eqe.2247

Permanent City Research Online URL: http://openaccess.city.ac.uk/3549/

A COMBINED LOCAL DAMAGE INDEX FOR SEISMIC ASSESSMENT OF EXISTING RC STRUCTURES

P. E. Mergos[1], A. J. Kappos[2]

[1] Lecturer, Technological Educational Institute of Chalkida, Chalkida, 34100 Greece
Former Graduate Student, Aristotle University of Thessaloniki, 54124 Greece
(tel: +30 22210 28329, e-mail: panmerg@yahoo.com)
[2] Professor, Lab. of Concrete and Masonry Structures, Department of Civil Engineering,
Aristotle University of Thessaloniki, 54124 Greece
(tel: +30 2310 995743, e-mail: ajkap@civil.auth.gr)

SUMMARY

A new local damage index for existing reinforced concrete (RC) structures is introduced, wherein deterioration caused by all deformation mechanisms (flexure, shear, anchorage slip) is treated separately for each mechanism. Moreover, the additive character of damage arising from the three response mechanisms, as well as the increase in degradation rate caused by their interaction, are fully taken into consideration. The proposed local damage index is then applied, in conjunction with a finite element model developed previously by the authors, to assess seismic damage response of several RC column and frame test specimens with substandard detailing. It is concluded that in all cases and independently from the prevailing mode of failure, the new local damage index describes well the damage pattern of the analysed specimens.

Keywords: Reinforced concrete, damage index, substandard detailing, flexure, shear, bond-slip

INTRODUCTION

In Greece as well as in other countries often struck by devastating earthquakes, a large fraction of the existing RC building stock has not been designed to conform to modern seismic codes. These structures have not been detailed in a ductile manner and according to capacity design principles. Therefore, it is likely, that in case of a major seismic event, their structural elements will suffer from brittle types of failure, which may lead to irreparable damage or collapse of the entire structure.

The first step in performing a realistic seismic damage analysis is to develop an analytical model that is able to predict accurately inelastic response during a seismic event. The complexity of this problem increases significantly for non-ductile RC structures, where, apart from flexure, shear and anchorage slip may significantly influence the final response. This is the reason why, for these structures, all three deformation mechanisms (flexure, shear, anchorage slip) should be properly treated, while their interaction should also be taken into consideration.

Only a small number of researchers [1-4] have applied numerical models for seismic assessment of non-ductile RC structures, where all three deformation mechanisms are considered individually. The authors [5-8] have developed a finite element capable of reproducing all three inelastic deformation mechanisms in an

explicit manner. This model is able to follow gradual spread of inelastic flexural and shear deformations as well as their interaction in the end regions of RC members. In addition, it has the ability of predicting shear failures caused by degradation of shear strength in the plastic hinge regions of RC elements, as well as bond types of failure caused by inadequate anchorage of the reinforcement in the joint regions or insufficient lap splice lengths. Hence, it can be considered as a reliable tool for seismic assessment of RC structures with substandard detailing.

The second step for a complete seismic damage analysis is to quantify numerically the level of structural damage caused by an earthquake. A large number of seismic damage indices have been proposed in the literature, reviewed in [9-10]. The level of sophistication of the existing damage indicators varies from the simple and traditional displacement ductility to cumulative damage models which attempt to take into account damage caused by repeated cycling. A major drawback of existing indices is that they have been formulated and verified almost exclusively on the basis of flexural damage mechanisms, possibly combining shear and bond-slip related mechanisms to the above, within the same constitutive law, e.g. moment-rotation [11]. Following this approach, the contribution of each deformation mechanism to the total damage of a critical area of a member will be proportional to the participation of the rotation caused by this mechanism to the total rotation of this area. This may underestimate significantly damage arising from relatively stiff deformation mechanisms, which contribute imperceptibly to the total rotation of the member. Furthermore, member end chord-rotation response cannot be determined a-priori in the general case, where the point of contraflexure shifts throughout the response.

Williams et al. [12] evaluated eight existing damage indices through comparison with a series of single-component tests using a variety of moment to shear ratios and stirrup spacing. They found that none of the proposed indices followed a clear shear-dependent trend.

The authors have proposed [13] a local damage index that incorporates seismic damage caused by inelastic shear and flexural deformations, as well as their interaction in an explicit manner. This index was able to reproduce the additive character of damage caused by shear and flexure and to provide reliable predictions of failure in flexure or shear. Nevertheless, this index has not been calibrated yet versus sufficient experimental data.

Until today, none of the existing damage indices has been developed to deal explicitly with bond deterioration and slippage of the reinforcement in the joint or lap splice regions. This contradicts the well-documented experimental observation [14, 15], that deficient anchorage or lap-splice detailing (insufficient embedment lengths, reinforcement cover, sparse transverse reinforcement, smooth bars and inadequate hooks) may cause severe damage leading to splitting of the surrounding concrete or reinforcement pullout.

In the following sections, the proposed analytical model for seismic damage assessment of RC structures with non-ductile detailing is presented. Initially, the finite element developed by the authors for the purposes of seismic response assessment is briefly described. Based on this finite element, a new local damage index is developed and calibrated for damage quantification in the critical end regions of RC members with substandard detailing. Finally, the derived analytical model is applied to seismic damage analysis of RC column and frame test specimens susceptible to different types of failure. The analytical predictions are compared with the experimental evidence.

FINITE ELEMENT MODEL

The finite element model [6-8] adopted herein for seismic damage analysis of existing RC structures is based on the flexibility approach (force-based element) and belongs to the class of phenomenological models. It consists of three sub-elements representing flexural, shear, and anchorage slip response (Fig. 1). The total flexibility of the finite element is calculated as the sum of the flexibilities of its sub-elements and can be inverted to produce the element stiffness matrix.

The flexural sub-element (Fig. 1c) is used for modelling flexural behaviour of an RC member before and after yielding of the longitudinal reinforcement. It consists of a set of rules governing the hysteretic moment-curvature (M-φ) response of the member end sections and a spread inelasticity model describing flexural stiffness distribution along the entire member [6].
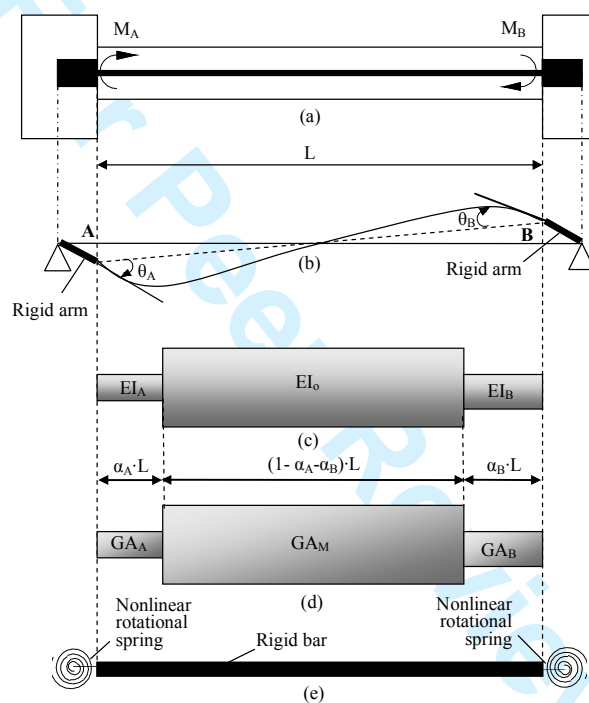
Figure 1: Proposed finite element model: a) geometry of RC member; b) beam-column finite element with rigid offsets; c) flexural sub-element; d) shear sub-element, e) anchorage bond-slip sub-element.

The M-φ hysteretic model is composed by the skeleton curve and a set of rules determining response during loading, unloading, and reloading. The M-φ envelope curve is derived by section analysis and appropriate bilinearization [8] with corner points corresponding, as a rule, to yielding and failure. Curvature capacity φ_u is considered as the minimum value from those corresponding to hoop fracture due to strain arising from the expansion of the concrete core [16], buckling of the longitudinal reinforcement [17], strength degradation exceeding 20% of the maximum moment capacity, and fracture of the tension reinforcement in the tension zone. Loading response is assumed to follow the bilinear envelope curve. Unloading is characterized by mild stiffness degradation; this is achieved by setting the unloading parameter of the Sivaselvan and Reinhorn [18] hysteretic model equal to 15.

Reloading aims at the point with previous maximum excursion in the opposite direction [6, 8].

To capture variation of section flexural stiffness along the concrete member, a gradual spread inelasticity model is adopted [19] as shown in Fig. (1c), where L is the length of the member; EI_A and EI_B are the current flexural rigidities of the sections at the ends A and B, respectively; EI_o is the elastic stiffness in the intermediate part of the element; α_A and α_B are the yield penetration coefficients. The flexural rigidities EI_A and EI_B are determined from the M-φ hysteretic relationship of the corresponding end sections. The yield penetration coefficients specify the proportion of the element where the acting moment is greater than the end-section yield moment. These coefficients are first calculated for the current moment distribution and then compared with the previous maximum penetration lengths [6, 8].

The shear sub-element models the hysteretic shear behaviour of the RC member prior and subsequent to shear cracking, flexural yielding and yielding of the transverse reinforcement. This sub-element has been designed in a similar way to the flexural element described above. It consists of a hysteretic model determining V-γ (shear force vs. shear deformation) behaviour of the member ends and/or intermediate regions and a shear spread-plasticity model determining distribution of shear stiffness along the RC member [6, 8].

Shear hysteresis is modelled using the V-γ skeleton curve described subsequently and the empirical hysteretic model by Ozcebe & Saatcioglu [20] and appropriate modifications introduced by the writers of this study [5]. The primary (skeleton) curve is first determined without considering shear-flexure interaction. This initial envelope curve (Fig. 2b) is valid for modelling shear behaviour outside the plastic hinge region for members that have yielded in flexure, or the response of the entire element for members, where the longitudinal reinforcement remains in the elastic range.
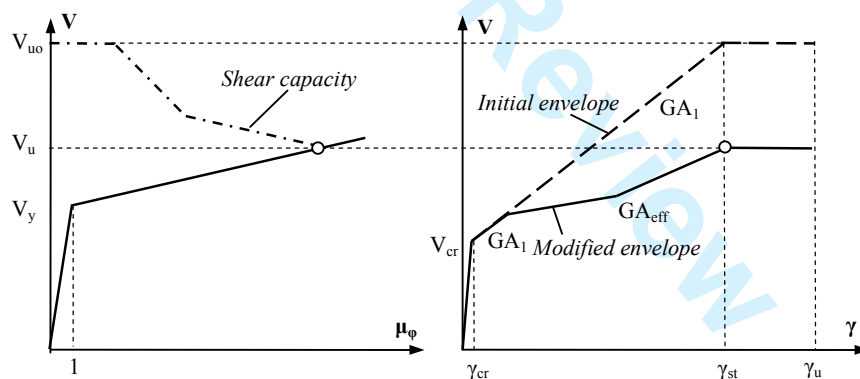
Figure 2: a) Flexural primary curve in terms of member shear force and curvature ductility demand of the critical cross section; b) shear (V – γ) primary curve before and after modelling shear-flexure interaction

The V-γ initial primary curve consists of four branches (Fig. 2), but only three different slopes, as explained later on. The first branch connects the origin and the shear cracking point, which is defined as the point where the nominal principal tensile stress exceeds the tensile strength of concrete. The second and third branches of the primary curve have the same slope and connect the shear cracking point (γ_{cr}, V_{cr}) to the point corresponding to the onset of yielding of transverse reinforcement, or else the point of attainment of maximum shear strength (γ_{st}, V_{uo}). The second and third branches are separated at the point corresponding to flexural yielding (γ_y, V_y). The

fourth branch is almost horizontal (stiffness close to zero) and extends up to the point of onset of shear failure (γ_u, V_{uo}).

Shear strain γ_{st} is calculated by the respective shear strain γ_{truss} calculated by the truss analogy approach [21], for an angle between the element axis and the concrete compression struts $\theta=45^o$, and two modification factors proposed by the authors [6] to account for member aspect ratio and normalized axial load. Hence, it is

$$\gamma_{st} = \kappa \cdot \lambda \cdot \gamma_{truss} \tag{1a}$$

$$\kappa = 1 - 1.07 \cdot v \tag{1b}$$

$$\lambda = 5.37 - 1.59 \cdot \min\left(2.5, \frac{L_s}{h}\right) \tag{1c}$$

Shear strain γ_u is calculated from an empirical formula proposed by the authors [7] on the basis of experimental data from 25 RC specimens failing in shear. The equations for determining γ_u are

$$\gamma_u = \lambda_1 \cdot \lambda_2 \cdot \lambda_3 \cdot \gamma_{st} \geq \gamma_{st} \tag{2a}$$

$$\lambda_1 = 1.0 - 2.5 \cdot \min\left(0.40, v\right) \tag{2b}$$

$$\lambda_2 = \min\left(2.5, L_s / h\right)^{2.0} \tag{2c}$$

$$\lambda_3 = 0.31 + 17.8 \cdot \min\left(\omega_\kappa, 0.08\right) \tag{2c}$$

$$\omega_\kappa = \frac{A_{sw} \cdot f_{yw}}{b \cdot s \cdot f_c} \tag{2d}$$

In the equations above, v is the normalized axial load, L_s and h the shear span and column depth, A_{sw} is the area of the transverse reinforcement oriented parallel to the applied shear force, b and s are the column width and stirrup spacing and f_{yw} and f_c are the yield strength of the transverse reinforcement and the concrete compressive strength respectively.

It is well documented [22] that shear strength of concrete resisting mechanisms V_c degrades due to disintegration of the plastic hinge zones caused by inelastic flexural deformations. Additionally, it has been shown experimentally [20] that shear strains increase rapidly in plastic hinge regions following flexural yielding. This combined phenomenon is characterized in the following as shear-flexure interaction effect.

The authors [5-8] have developed a methodology for defining the V-γ envelope curve incorporating interaction with flexure. According to this procedure, the shear strain γ after flexural yielding and prior to stirrup yielding is given by Eq. (3), where GA_1 is the cracked shear stiffness of the initial envelope given by Eq. (4), V_{st} is the shear force carried by the transverse reinforcement, V is the applied shear force and $degV_c$ is the total drop in the concrete mechanism shear strength capacity V_c for the curvature ductility demand μ_φ corresponding to V. $degV_c$ may be determined by a shear strength model accounting for degradation of V_c with μ_φ, such as the one described in [22]. It is noted that at stirrup yielding, it becomes $V_{st}=V_w$, where V_w is the shear strength capacity of the transverse reinforcement.

$$\gamma = \gamma_{cr} + \frac{V_{st}}{GA_1} = \gamma_{cr} + \frac{V - V_{cr} + \deg V_c}{GA_1} \tag{3}$$

$$GA_1 = \frac{V_{uo} - V_c}{\gamma_{st} - \gamma_{cr}}$$ (4)

Fig. 2 compares the initial V-γ envelope curve and the 'modified' one derived from Eq. (3) for the case of a shear-flexure critical cantilever column. It is evident that, for the same shear force demand, shear strains from the 'modified' envelope result significantly higher than the initial envelope after yielding in flexure. It is worth noting that stirrup yielding occurs for the 'modified' envelope again at shear strain γ_{st} in accordance with the truss-analogy approach. After stirrup yielding, both envelopes follow an almost horizontal branch [8].

To adequately capture shear stiffness variation along the concrete member, a shear spread inelasticity model is adopted, as first introduced by the authors of this study [6-8]. As shown in Fig. (1d), the shear spread inelasticity model is composed from two end-zones, where flexural yielding takes place and an intermediate zone determining the rest of the member. The end-zones have variable lengths equal to the lengths of the respective inelastic zones of the flexural sub-element and stiffness determined from the 'modified' envelope curve for the respective μ_φ of the flexural sub-element. The stiffness of the intermediate region is defined on the basis of the initial V-γ envelope curve.

The bond-slip sub-element accounts for the fixed-end rotations (θ_{sl}) which arise at the interfaces of adjacent RC members due to bond deterioration and slippage of the reinforcement in the joint regions and the lap splices. The proposed model consists of two concentrated rotational springs located at the member ends [6, 8]. The two (uncoupled) springs are connected by an infinitely rigid bar (Fig. 1e).

The M-θ_{sl} skeleton curve is derived on the basis of a simplified procedure [23] assuming uniform bond stress along different segments of the anchored rebar. These segments are the elastic region, the strain-hardening region and the cone penetration zone. The average elastic bond strength τ_{be} according to ACI 408 [24] is adopted here for the elastic region, while the frictional bond τ_{bf} of the CEB Model Code [25] is assumed to apply within the strain-hardening region. In the cone penetration zone, it is assumed that bond stress is negligible.

Based on these assumptions, reinforcement slippage δ_{sl} is calculated for each step of end section M-φ analysis by integrating rebar strains along the anchorage length. Then, by dividing δ_{sl} by the distance of the anchored bar to the neutral axis depth, the respective fixed-end rotation θ_{sl} is determined.

The envelope M-θ_{sl} curve defined by the various points of the afore-described methodology is then idealized by a bilinear relationship with the corner points corresponding to yielding and failure. After defining M-θ_{sl} bilinear envelope, bond-slip hysteresis is modelled following the suggestions of Saatcioglu and Alsiwat [26].

For straight and hooked anchorages, the fixed end rotation corresponding to anchorage failure $\theta_{ub,sl}$ may be determined by the analytical methodology by Alsiwat and Saatcioglu [23] for the point corresponding to 20% drop in the maximum anchorage moment capacity. It is worth noting, that for well detailed anchorages, bond failure may not take place prior to fracture of the tensile reinforcement. In these cases, fixed-end rotation $\theta_{ub,sl}$ is assumed herein as the one corresponding to fracture of tensile reinforcement. Nevertheless, it is emphasized that in RC structures with sub-standard detailing, it is very likely that bond failures precede the development of flexural modes of failure.

In the presence of lap splices, additional fixed-end rotations arising from slippage of the reinforcement in the splice regions should be added to θ_{sl} [27]. A very common deficiency in under-designed RC structures is the existence of very short lap splices in the locations of the potential plastic hinges. These splices were designed solely for compression. Hence, under tension loading imposed by earthquakes, these splices frequently fail prior to yielding of the longitudinal reinforcement.

Melek et al. [15] investigated the experimental response of such column lap splices. They concluded that the average bond strength of these splices is approximately $u_{lap}=0.95\sqrt{f_c}$. This value is also adopted herein for determining ultimate moment capacity M_{lap} of inadequate lap splices.
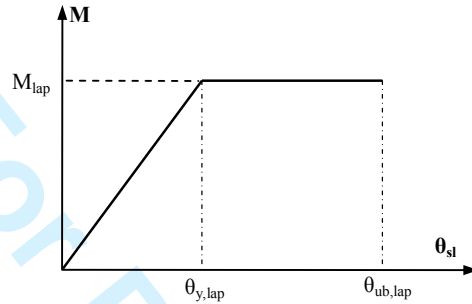

Figure 3: Bilinear approximation of the M-θ_{sl} response of RC member ends with poor lap splices.

Fixed-end rotation $\theta_{y,lap}$ corresponding to attainment of M_{lap} is determined by adding the respective fixed-end rotations developed along the anchorage and lap splice length. Fixed-end rotations arising from poor lap splices are determined by assuming uniform bond strength u_{lap} along the splice length. The fixed-end rotation $\theta_{ub,lap}$ corresponding to 20% drop in the lap splice moment capacity is determined by Eq. (5). This approximate equation was derived by investigating the experimental results of Melek el al. [15]. Further study is required in the future for more accurate prediction of $\theta_{ub,lap}$.

$$\theta_{ub,lap} = \theta_{y,lap} + 0.005 \tag{5}$$

LOCAL DAMAGE INDEX

General formulation

By definition, a seismic damage index is a quantity with zero value when no damage occurs and equal to 1 (100%), when failure occurs [9]. However, a non-ductile RC member may fail either in flexure or in shear or due to loss of bond (in an anchorage or lap-splice zone). Hence, an appropriate local seismic damage index, D_{tot}, for such a member should assume unity value when the respective end of the member reaches its flexural *or* shear *or* bond-slip deformation capacity. A general mathematical relationship that satisfies the aforementioned limitations is

$$D_{tot} = 1-\left(1-D_{fl}\right)^{\xi_{fl}} \cdot \left(1-D_{sh}\right)^{\xi_{sh}} \cdot \left(1-D_{sl}\right)^{\xi_{sl}} \tag{6}$$

where D_{tot} is the total local damage index ($0 \leq D_{tot} \leq 1$) representing total damage at the member end; D_{fl} is the flexural damage index ($0 \leq D_{fl} \leq 1$), representing flexural damage at the member end; D_{sh} is the shear damage index ($0 \leq D_{sh} \leq 1$) representing shear damage at the member end; D_{sl} is the bond slip damage index ($0 \leq D_{sl} \leq 1$) representing

bond slip damage at the member end; ξ_{fl} is an exponent related to the contribution of the flexural damage index D_{fl} to the total damage index D_{tot}; ξ_{sh} is an exponent related to the contribution of the shear damage index D_{sh} to the total damage index D_{tot} and ξ_{sl} is an exponent related to the contribution of the bond slip damage index D_{sl} to the total damage index D_{tot}. Eq. (6) is a straightforward extension of a similar formula proposed earlier by the authors [13] accounting only for shear and flexural failure.

In Eq. (6), when no flexural, shear or bond damage at the element end has occurred ($D_{fl}=D_{sh}=D_{sl}=0$) the total damage index D_{tot} remains equal to zero. However, if flexural failure occurs ($D_{fl}=1$) then D_{tot} becomes equal to unity independently from the values of the respective damage indices D_{sh} and D_{sl}. In a similar fashion, when shear failure takes place ($D_{sh}=1$), D_{tot} becomes equal to unity irrespective of the condition of the member end in terms of D_{fl} and D_{sl}. Finally, when bond-slip failure occurs ($D_{sl}=1$), D_{tot} becomes equal to unity irrespective of the condition of the member end in terms of D_{fl} and D_{sh}. The physical interpretation of this observation is that the RC member end has reached its capacity when either flexural, shear, or bond failure occurs, independently of the damage state in the other two deformation mechanisms.

Calculation of D_{tot}, as given by Eq. (6), can be strongly influenced by the values adopted in the analysis for the exponents ξ_{fl}, ξ_{sh} and ξ_{sl}. For example, if ξ_{max}, ξ_{int} and ξ_{min} are the exponents of the maximum D_{max}, intermediate D_{int} and minimum D_{min} values of the individual damage indices D_i (i= fl, sh, sl) respectively, then, by setting $\xi_{max}=1$ and $\xi_{int}=\xi_{min}=0$, it becomes $D_{tot}=D_{max}$. This would be compatible with a damage scale, where the total damage state is assumed equal to the damage state of the most critical mechanism. However, in this manner, the additional damage caused by the other two deformation mechanisms is neglected.

Furthermore, it is physically meaningful to assume that when two out of three types of damage (flexure, shear or bond) are negligible at the RC member end, the total damage in this end is equal to the damage caused by the third deformation mechanism. For example, if $D_{fl}=D_{sl}=0$, it is rational to assume that $D_{tot}=D_{sh}$. In Eq. (5) this can be achieved only when $\xi_{fl}=\xi_{sh}=\xi_{sl}=1$.

Based on the above considerations, Eq. (7) is finally proposed herein for determining D_{tot} from the individual damage indices D_{fl}, D_{sh} and D_{sl}.

$$D_{tot} = 1 - \left(1 - D_{fl}\right) \cdot \left(1 - D_{sh}\right) \cdot \left(1 - D_{sl}\right) \tag{7}$$
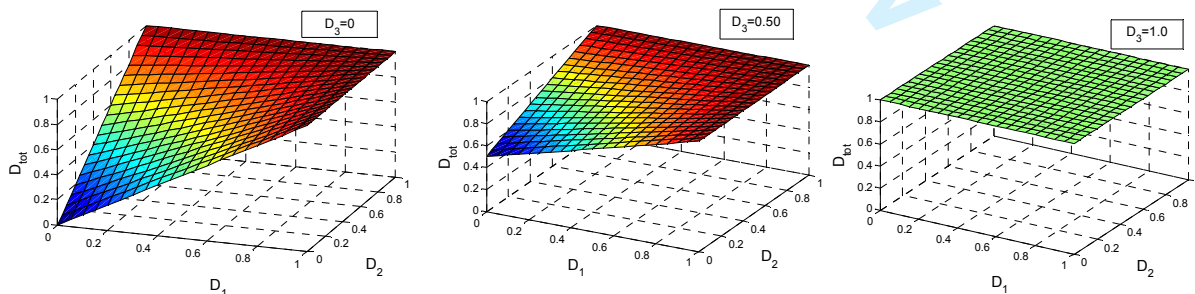
Figure 4: Variation of D_{tot} for different values of individual damage indices D_i (i=1,2,3)

Fig. (4) illustrates variation of D_{tot} for all possible combinations of individual damage indices D_1, D_2 and for three distinct values of the third index D_3, where every index D_i (i=1,2,3) corresponds to one of the indices D_{fl}, D_{sh} and D_{sl} in a random order. It can be seen that D_{tot} assumes a zero value when all indices D_i are equal to zero (no

damage in flexure, shear or bond). Furthermore, it is obvious that when one of the damage indices D_i becomes equal to one (flexural, shear of bond failure) then D_{tot} becomes equal to one as well, irrespective of the value of the other indices.

For all other intermediate values of D_i (i=1,2,3), D_{tot} becomes always equal or greater than D_{max}, where D_{max} is the maximum value of the individual indices D_i. In this way, the combined deterioration effect caused by the three individual damage mechanisms (flexure, shear, bond) is explicitly taken into account. More particularly, D_{tot} ranges between $D_{max} \leq D_{tot} \leq 1-(1-D_{max})^3$. The lower limit is valid when the other two individual indices D_i are equal to zero and the upper limit occurs when all indices D_i are equal to D_{max}.

It is evident that for the calculation of total damage index D_{tot} determination of individual damage indices D_{fl}, D_{sh} and D_{sl} is first required. In general, damage in RC elements is related to deformations. Therefore, any damage variable should preferably refer to a certain deformation quantity [9].

By definition, the flexural damage index D_{fl} should refer to a local, purely flexural, deformation variable. The best choice for this case is the curvature φ developed at the respective end of the member. In a similar fashion, shear damage index D_{sh} should refer to the shear distortion developed at the respective end region of the RC member. Lastly, bond-slip damage index D_{sl} has to be correlated with fixed-end rotation θ_{sl}.

Following the basic definition of a seismic damage index, D_{fl}, D_{sh} and D_{sl} must also have a zero value when no flexural, shear, or bond, damage takes place and they must be equal to unity when flexural, shear or bond failure occurs, respectively.

Flexural damage at an RC member end initiates when the maximum curvature developed φ_{max} at the respective end of the member exceeds a threshold value φ_o below which essentially elastic behaviour occurs, in the sense that no permanent deformation is visible and therefore no damage is detected. In an analogous fashion, shear and bond-slip damage at an RC member end takes place when maximum shear distortion γ_{max} or maximum fixed-end rotation $\theta_{sl,max}$ become greater than their respective threshold values γ_o and $\theta_{sl,o}$.

In addition, flexural failure develops at an RC member end when φ_{max} reaches the corresponding capacity φ_u. Similarly, shear failure may be assumed to develop when γ_{max} reaches the corresponding capacity γ_u and bond failure when $\theta_{sl,max}$ becomes equal to $\theta_{ub,sl}$. It is recalled that determination of available deformation capacities φ_u, γ_u and $\theta_{ub,sl}$ has already been described in the previous section of this paper.

Three general relationships for the flexural, shear and bond damage index, satisfying the aforementioned limitations, are the ones given in Eqs. (8).

$$D_{fl} = \left(\frac{\varphi_{max} - \varphi_o}{\varphi_u - \varphi_o} \right)^{\lambda_{fl}} \; ; D_{sh} = \left(\frac{\gamma_{max} - \gamma_o}{\gamma_u - \gamma_o} \right)^{\lambda_{sh}} \; ; D_{sl} = \left(\frac{\vartheta_{sl,max} - \vartheta_{sl,o}}{\vartheta_{ub,sl} - \vartheta_{sl,o}} \right)^{\lambda_{sl}} \qquad (8)$$

In these equations, λ_{fl}, λ_{sh} and λ_{sl} are exponents determining the rate at which flexural, shear, or bond, damage increases with the normalized ratios $(\varphi_{max}-\varphi_o)/(\varphi_u-\varphi_o)$, $(\gamma_{max}-\gamma_o)/(\gamma_u-\gamma_o)$ and $(\theta_{sl,max}-\theta_{sl,o})/(\theta_{ub,sl}-\theta_{sl,o})$, respectively. It is worth pointing out, that these normalized ratios represent special cases of Eqs (8) by setting $\lambda_{fl}=\lambda_{sh}=\lambda_{sl}=1$.

It is clear that in Eqs (8) when $\varphi_{max}<\varphi_o$ or $\gamma_{max}<\gamma_o$ or $\theta_{sl,max}<\theta_{sl,o}$ then $\varphi_{max}=\varphi_o$ and $\gamma_{max}=\gamma_o$ and $\theta_{sl,max}=\theta_{sl,o}$, respectively, should be introduced in the equations to avoid negative values for D_{tot}. Determination of D_{tot} can be influenced significantly by the definition of the threshold values φ_o, γ_o and $\theta_{sl,o}$ below which no damage is detected. Values corresponding to flexural and shear cracking or flexural, anchorage slip and shear yielding may be adopted. However, due to the nonlinear, inelastic behaviour of

RC from the very early stages of response, definition of φ_o, γ_o and $\theta_{sl,o}$ is not always straightforward. Furthermore, for a broad class of RC members, the aforementioned values represent only a very small fraction of φ_u, γ_u and $\theta_{ub,sl}$ respectively; hence, their inclusion in the determination of D_{tot} has only a minor influence on the results [13]. In this study, for simplification reasons, it is assumed that $\varphi_o=\gamma_o=\theta_{sl,o}=0$.

Taking the above into consideration, Eq. (9) is derived for D_{tot} determination.

$$D_{tot} = 1 - \left(1 - \left(\frac{\varphi_{max}}{\varphi_u}\right)^{\lambda_{fl}}\right) \cdot \left(1 - \left(\frac{\gamma_{max}}{\gamma_u}\right)^{\lambda_{sh}}\right) \cdot \left(1 - \left(\frac{\theta_{sl,max}}{\theta_{ub,sl}}\right)^{\lambda_{sl}}\right) \quad (9)$$

It is evident that the values of λ_{fl}, λ_{sh}, λ_{sl} may have a vital influence on the final outcome of D_{tot}. Clearly, these exponents should be determined on the basis of experimental evidence. An attempt to calibrate these values is made in the following section.

As a final consideration regarding damage index formulation, the issue of cumulative damage effect due to repeated loading should be addressed. Kappos and Xenos [28] assessed the importance of the energy term in the combined damage index of Park-Ang [11] considering realistic structures and hysteretic characteristics, realistic seismic inputs, and also a sufficiently rigorous dynamic inelastic analysis procedure. It was found that the contribution of the energy term to the value of the damage index is very low for the case of well-detailed RC members. However, for RC members with poor detailing available data remains ambiguous since calibration against experimental evidence is still very limited.

Eq. (9) can be easily extended to include cumulative damage effects. To this purpose, Eq. (10) is proposed herein, which has been inspired by a similar proposal made by Mehanny and Deierlein [29] for inelastic chord rotations.

$$D_{tot} = 1 - \left(1 - \frac{\varphi_{max}^{\lambda_{fl}} + \left(\sum\limits_{i=1}^{n}\varphi_i\right)^{\beta_{fl}}}{\varphi_u^{\lambda_{fl}} + \left(\sum\limits_{i=1}^{n}\varphi_i\right)^{\beta_{fl}}}\right) \cdot \left(1 - \frac{\gamma_{max}^{\lambda_{sh}} + \left(\sum\limits_{i=1}^{n}\gamma_i\right)^{\beta_{sh}}}{\gamma_u^{\lambda_{sh}} + \left(\sum\limits_{i=1}^{n}\gamma_i\right)^{\beta_{sh}}}\right) \cdot \left(1 - \frac{\theta_{sl,max}^{\lambda_{sl}} + \left(\sum\limits_{i=1}^{n}\theta_{sl,i}\right)^{\beta_{sl}}}{\theta_{ub,sl}^{\lambda_{sl}} + \left(\sum\limits_{i=1}^{n}\theta_{sl,i}\right)^{\beta_{sl}}}\right) \quad (10)$$

In this equation, φ_u, γ_u and $\theta_{ub,sl}$ represent ultimate deformation capacities under monotonic loading. In addition, φ_{max}, γ_{max} and $\theta_{sl,max}$ represent maximum deformations in the critical direction of loading, while φ_i, γ_i and $\theta_{sl,i}$ refer to maximum (vertex) deformations of all subsequent n cycles of smaller amplitude in the same direction of loading.

In Eq. (10), β_{fl}, β_{sh} and β_{sl} are exponents expressing the importance of cyclic damage accumulation to the total damage of the member end for the respective type of deformation. Again these values should be determined on the basis of experimental evidence. Nevertheless, to the authors' opinion, available experimental data is far from sufficient to provide reliable predictions for these exponents. Hence, for the sake of simplicity and clarity, Eq. (9) is adopted in the remainder of this paper and cyclic loading effects are taken into consideration indirectly as explained later on in the damage index calibration procedure. Further study is required in the future for determining more accurately cumulative damage effects, especially in the case of structures with substandard detailing.

Damage index calibration

The calibration of the proposed damage index includes the determination of the exponent parameters λ_{fl}, λ_{sh} and λ_{sl} of Eq. (9). As mentioned above, these parameters express the rate of flexural, shear, and bond damage progression of the RC member end with the normalized ratios φ_{max}/φ_u, γ_{max}/γ_u and $\theta_{sl,max}/\theta_{ub,sl}$, respectively.

Flexural damage in RC members refers to flexural cracking, spalling of the cover concrete and, in the final state, buckling of the compression reinforcement, fracture of the tensile reinforcement, core concrete disintegration, and yielding or fracture of transverse reinforcement due to concrete core expansion.

Shear damage develops through inclined-shear cracking that propagates as the level of shear force carried by the truss mechanism increases. In the final state, stirrup yielding takes place followed by severe shear cracking and the inability of the RC member to withstand the acting shear force.

For columns without lap splices, bond damage is defined herein as the fixed-end cracks developed due to reinforcement slippage in the adjacent joints. These cracks have the same form and are often confused with flexural cracking, but they are developed due to anchorage slippage in the joint regions.

In the case of inadequate lap splices, the development of bond cracks in the direction of the lap-spliced bars is also taken into consideration. Substandard lap splices tend to fail after the appearance of wide bond cracks along the full length of the splices, followed by spalling of the cover concrete surrounding the spliced bars.

The first step to calibrate the damage index coefficients is to define an appropriate damage scale for each type of structural damage. The damage scales adopted herein for each deformation mechanism are presented in Table 1.

Three different damage levels are considered. Damage Level (A) characterizes element response from no-damage to minor damage condition. This Damage Level could be associated with the Immediate Occupancy Structural Performance Level of FEMA-356 [30] Guidelines. The shear cracking width (0.5 mm) threshold for this Damage Level is taken from the EPPO [31] (Earthquake Planning and Protection Organization of Greece) respective damage scale, set up on the basis of observed damage in several earthquakes in Greece. Regarding bond cracking in the lap splices, the general procedure of paragraph §2.8 of FEMA-356 Guidelines is applied, which refers to experimentally obtained cyclic response characteristics. According to this paragraph, the Immediate Occupancy Level is defined by the deformation at which permanent and visible damage occurred during the experiments.

The second Damage Level (B) covers element response ranging from minor damage to severe damage. Despite the fact that damage becomes significant during this range of response, the lateral force carrying capacity of all deformation mechanisms continues to increase with increasing deformations. The end of this Damage Level corresponds to attainment of the respective (flexural, shear or bond) maximum strength capacity.

The third and final Damage Level (C) is accompanied by severe structural damage for each deformation mechanism. Over this range of response, the RC member is no longer able to increase its strength capacity. Hence, the lateral capacity of all deformation mechanisms begins to drop gradually with increasing deformation demand or it remains marginally stable and then drops suddenly. In all cases, the end deformation limit for Damage Level (C) is taken herein as the deformation corresponding to 20% loss in the respective maximum strength capacity. This is in accordance with the definitions of the ultimate deformation capacities φ_u, γ_u and $\theta_{ub,sl}$ given in the previous paragraphs.

The thresholds separating moderate and severe damage responses were derived by investigating the experimental response of 12 well-documented column specimens with different modes of failure used later on to calibrate the proposed damage index.

The second step of the damage index calibration process is the correlation of the damage index values to the damage scales described above. One way to achieve this is to pre-select the damage index parameters (i.e. exponents λ_{fl}, λ_{sh} and λ_{sl}) and then perform seismic damage analyses in order to correlate the outcome of the damage indices with the observed structural damage. The drawback of this approach is that, if inappropriate values for the damage index parameters are chosen, then distinction between the various damage levels from the damage index results is not always clear, also taking into consideration the large amount of uncertainty characterising these quantities.

To overcome this problem, an alternative approach is adopted herein. According to this, the damage index values corresponding to the different damage levels are defined a-priori with a view to providing clear distinction among the individual damage states. Then, damage analyses are performed with the damage parameters (λ_{fl}, λ_{sh} and λ_{sl}) kept as unknowns. Finally, regression analyses are carried out, to achieve maximum correlation of the damage index results with the observed damage.

The damage index values adopted in this study to represent the different levels of the damage scale are shown in Table 1. However, it should be clear that the methodology applied later on for calibrating the proposed damage model may be easily adjusted to different index values, whenever required.

Table 1. Adopted scale for flexural, shear and bond damage mechanisms of RC member critical regions.

Damage Level	Flexural damage	Shear damage	Bond damage	Damage Index
(A) Minor damage	Flexural cracks (<2 mm). Limited yielding. No spalling.	Hairline-minor shear cracks (<0.5 mm)	Fixed-end cracks (<2 mm). Hairline – visible bond cracks in parts of the lap splices	0.00-0.20
(B) Moderate damage	Spalling of concrete cover	Moderate shear cracking (>0.5 mm)	Fixed-end cracks (>2 mm). Moderate bond cracking in parts of the lap splices	0.20-0.50
(C) Severe damage	Buckling of compressive reinforcement, core concrete disintegration, fracture of tensile reinforcement, yielding or fracture of transverse reinforcement due to core expansion.	Severe shear cracking (>1 mm), stirrup yielding or fracture.	Major fixed-end cracks indicating reinforcement pullout. Severe bond cracking along the full length of the lap splices. Spalling of cover surrounding lap-spliced bars	0.50-1.00

The adopted calibration procedure is applied to 12 RC column specimens that experienced different types of failure. For all of these specimens a detailed description of their damage progression is available, something not common in the pertinent literature. Four of them developed flexural failures, four failed in shear mode and four of them experienced bond-slip type of failure. The latter failed due to bond deterioration of their deficient lap splices [15]. The column specimens, as well as their modes of failure, are reported in Table 2.

First, the ultimate deformation capacities of these elements φ_u, γ_u and $\theta_{ub,sl}$ are calculated based on the analytical procedures described earlier in this study and they are presented in Table 2.

In addition, for each specimen, displacement-controlled pushover analysis is conducted up to the level of experimental lateral displacement ductility $\mu_{\Delta u}$ corresponding to the onset of significant lateral strength degradation ($D_{tot}=1.0$), by applying the finite element model described in the previous chapter of this paper. The pushover analysis calculated normalized deformation ratios φ/φ_u, γ/γ_u and $\theta_{sl}/\theta_{ub,sl}$ for different levels of the imposed ductility demands μ_Δ are summarized in Table 2. The ductility levels μ_Δ given in column 4 of Table 2 correspond to those displacement ductilities at which the experimental researchers provided analytical descriptions of the specimen damage state. For the bond-critical specimens [15], the value in the same column of Table 2 refers to the imposed lateral drift (%). This is because no flexural yielding occurred during these experiments and displacement ductility could not be defined.

Table 2. Calibration of damage index D_{tot}

Speci-men	Ref	Mode of failure	μ_Δ or drift (%)	φ_u (m⁻¹)	γ_u	$\theta_{ub,sl}$ (rad)	φ/φ_u	γ/γ_u	$\theta_{sl}/\theta_{ub,sl}$	D_{fl}^{exp}	D_{sh}^{exp}	D_{sl}^{exp}
415	[32]	F	1.0	0.200	0.033	0.064	0.08	0.01	0.04	0.10	0.10	0.10
415	[32]	F	2.0	0.200	0.033	0.064	0.28	0.04	0.12	0.20	0.10	0.20
415	[32]	F	3.0	0.200	0.033	0.064	0.47	0.05	0.20	0.40	0.10	0.30
415	[32]	F	5.0	0.200	0.033	0.064	0.80	0.05	0.34	0.60	0.10	0.30
415	[32]	F	7.0	0.200	0.033	0.064	1.09	0.05	-	1.00	0.10	N/R
407	[32]	F	0.9	0.220	0.033	0.064	0.03	0.00	0.02	0.10	0.00	0.10
407	[32]	F	1.3	0.220	0.033	0.064	0.10	0.00	0.04	0.10	0.00	0.20
407	[32]	F	2.0	0.220	0.033	0.064	0.23	0.03	0.08	0.20	0.10	0.20
407	[32]	F	3.0	0.220	0.033	0.064	0.41	0.04	0.14	0.40	0.10	0.30
407	[32]	F	6.0	0.220	0.033	0.064	0.85	0.04	0.28	1.00	0.10	0.40
430	[32]	F	1.0	0.166	0.033	0.064	0.06	0.02	0.02	0.10	0.10	0.10
430	[32]	F	1.5	0.166	0.033	0.064	0.14	0.03	0.06	0.10	0.10	0.10
430	[32]	F	2.0	0.166	0.033	0.064	0.24	0.04	0.11	0.20	0.10	0.30
430	[32]	F	3.0	0.166	0.033	0.064	0.43	0.06	0.20	0.30	0.10	0.30
430	[32]	F	5.0	0.166	0.033	0.064	0.77	0.07	-	0.40	0.10	N/R
430	[32]	F	7.0	0.166	0.033	0.064	1.08	0.08	-	1.00	0.10	N/R
815	[32]	F	1.0	0.200	0.033	0.064	0.08	0.00	0.04	0.10	0.00	0.10
815	[32]	F	1.5	0.200	0.033	0.064	0.21	0.00	0.09	0.10	0.00	0.30
815	[32]	F	2.0	0.200	0.033	0.064	0.32	0.00	0.14	0.20	0.00	0.30
815	[32]	F	3.0	0.200	0.033	0.064	0.53	0.00	-	0.40	0.00	N/R
815	[32]	F	5.0	0.200	0.033	0.064	0.88	0.00	0.37	1.00	0.00	0.40
No 1	[33]	S	0.5	0.045	0.012	-	0.11	0.02	-	0.10	0.20	N/R
No 1	[33]	S	1.0	0.045	0.012	-	0.22	0.13	-	0.10	0.30	N/R
No 1	[33]	S	2.0	0.045	0.012	-	0.44	0.23	-	0.40	0.50	N/R
No 1	[33]	S	3.0	0.045	0.012	-	0.67	1.19	-	0.50	1.00	N/R
No 4	[33]	S	0.5	0.045	0.012	-	0.11	0.02	-	0.10	0.10	N/R
No 4	[33]	S	1.0	0.045	0.012	-	0.22	0.13	-	0.10	0.20	N/R
No 4	[33]	S	2.0	0.045	0.012	-	0.44	0.23	-	0.30	N/R	N/R
No 4	[33]	S	3.0	0.045	0.012	-	0.67	1.19	-	0.40	1.00	N/R
HS2	[34]	S	0.5	0.049	0.013	-	0.04	0.05	-	0.10	0.10	N/R
HS2	[34]	S	.75	0.049	0.013	-	0.05	0.12	-	0.10	0.20	N/R
HS2	[34]	S	1.0	0.049	0.013	-	0.06	0.15	-	0.10	0.30	N/R
HS2	[34]	S	1.5	0.049	0.013	-	0.23	0.22	-	0.20	0.40	N/R
HS2	[34]	S	2.0	0.049	0.013	-	0.35	0.32	-	0.30	0.40	N/R

HS2	[34]	S	3.0	0.049	0.013	-	0.43	0.39	-	0.50	0.50	N/R
HS2	[34]	S	3.5	0.049	0.013	-	0.45	1.22	-	0.60	1.00	N/R
HS3	[34]	S	0.5	0.013	0.007	-	0.14	0.12	-	0.10	0.10	N/R
HS3	[34]	S	.75	0.013	0.007	-	0.21	0.21	-	0.10	0.20	N/R
HS3	[34]	S	1	0.013	0.007	-	0.28	0.32	-	0.20	0.30	N/R
HS3	[34]	S	1.5	0.013	0.007	-	0.54	0.36	-	0.40	0.60	N/R
HS3	[34]	S	2.0	0.013	0.007	-	0.85	0.71	-	0.70	1.00	N/R
S10MI	[15]	B	.25	0.062	0.011	0.010	0.04	0.00	0.11	0.10	0.10	0.10
S10MI	[15]	B	.75	0.062	0.011	0.010	0.11	0.01	0.34	0.10	0.10	0.20
S10MI	[15]	B	1.0	0.062	0.011	0.010	0.13	0.05	0.43	0.10	0.10	0.20
S10MI	[15]	B	1.5	0.062	0.011	0.010	0.15	0.09	0.83	0.10	0.10	0.50
S10MI	[15]	B	2.0	0.062	0.011	0.010	0.16	0.10	1.30	0.10	0.10	1.00
S20MI	[15]	B	.25	0.053	0.003	0.010	0.04	0.01	0.11	0.10	0.10	0.10
S20MI	[15]	B	.75	0.053	0.003	0.010	0.12	0.02	0.33	0.10	0.20	0.20
S20MI	[15]	B	1.0	0.053	0.003	0.010	0.16	0.10	0.44	0.10	0.20	0.50
S20MI	[15]	B	1.5	0.053	0.003	0.010	0.19	0.28	0.78	0.10	0.30	0.70
S20MI	[15]	B	2.0	0.053	0.003	0.010	0.20	0.31	1.24	0.10	0.30	1.00
S30MI	[15]	B	0.5	0.033	0.003	0.011	0.13	0.02	0.21	0.10	0.10	0.10
S30MI	[15]	B	.75	0.033	0.003	0.011	0.20	0.03	0.31	0.10	0.20	0.10
S30MI	[15]	B	1.5	0.033	0.003	0.011	0.34	0.30	0.66	0.10	0.20	0.50
S30MI	[15]	B	1.8	0.033	0.003	0.011	0.34	0.32	0.92	0.10	0.20	1.00
S30XI	[15]	B	.25	0.033	0.003	0.011	0.07	0.01	0.11	0.10	0.10	0.10
S30XI	[15]	B	0.5	0.033	0.003	0.011	0.14	0.02	0.22	0.10	0.10	0.10
S30XI	[15]	B	.75	0.033	0.003	0.011	0.22	0.04	0.34	0.10	0.20	0.20
S30XI	[15]	B	1.5	0.033	0.003	0.011	0.34	0.54	0.71	0.10	0.30	0.60
S30XI	[15]	B	2.0	0.033	0.003	0.011	0.35	0.57	1.15	0.10	0.30	1.00

F=flexure; S=Shear; B=Bond; N/R=Not Recorded; the drift (%) values of column 4 correspond to specimens of reference [15].

Moreover, following the experimental observations regarding all damage modes (flexure, shear, bond) for all RC specimens and imposed displacement ductilities (drifts), the experimental individual damage indices D_{fl}^{exp}, D_{sh}^{exp}, D_{sl}^{exp} are estimated in accordance with the damage scales described in Table 1. It is important to mention here that the experimental damage index values have been derived from the final loading cycle at each imposed ductility (drift) level. In this way, additional degradation due to cyclic loading effects is taken indirectly into account in the analytical procedure.

Having established the experimental D_{fl}^{exp}, D_{sh}^{exp} and D_{sl}^{exp} values for the different calculated normalized ratios φ/φ_u, γ/γ_u and $\theta_{sl}/\theta_{ub,sl}$, nonlinear regression analyses are conducted to evaluate the values of λ_{fl}, λ_{sh} and λ_{sl}, which provide maximum correlation between the predicted by Eqs (8) D_{fl}^{pred}, D_{sh}^{pred}, D_{sl}^{pred} damage index values and their experimental counterparts. Based on these analyses, values of exponents λ_{fl}, λ_{sh} and λ_{sl} are found to be equal to 1.35, 0.95 and 0.80 respectively. The correlation derived by these values between D_i^{exp} and D_i^{pred} (i=fl, sh, sl) is illustrated in Fig. (5). The coefficient of determination R^2 is found to be 0.86, 0.79 and 0.73, respectively. These values can be deemed as satisfactory considering the complexity and uncertainty inherent to this problem. Nevertheless, it must be recalled that the sample used for this study remains quite small (the reason being the unavailability of test reports with detailed description of the development of damage with increasing imposed displacement) and additional statistical analyses are required in the future to attain more reliable solutions.
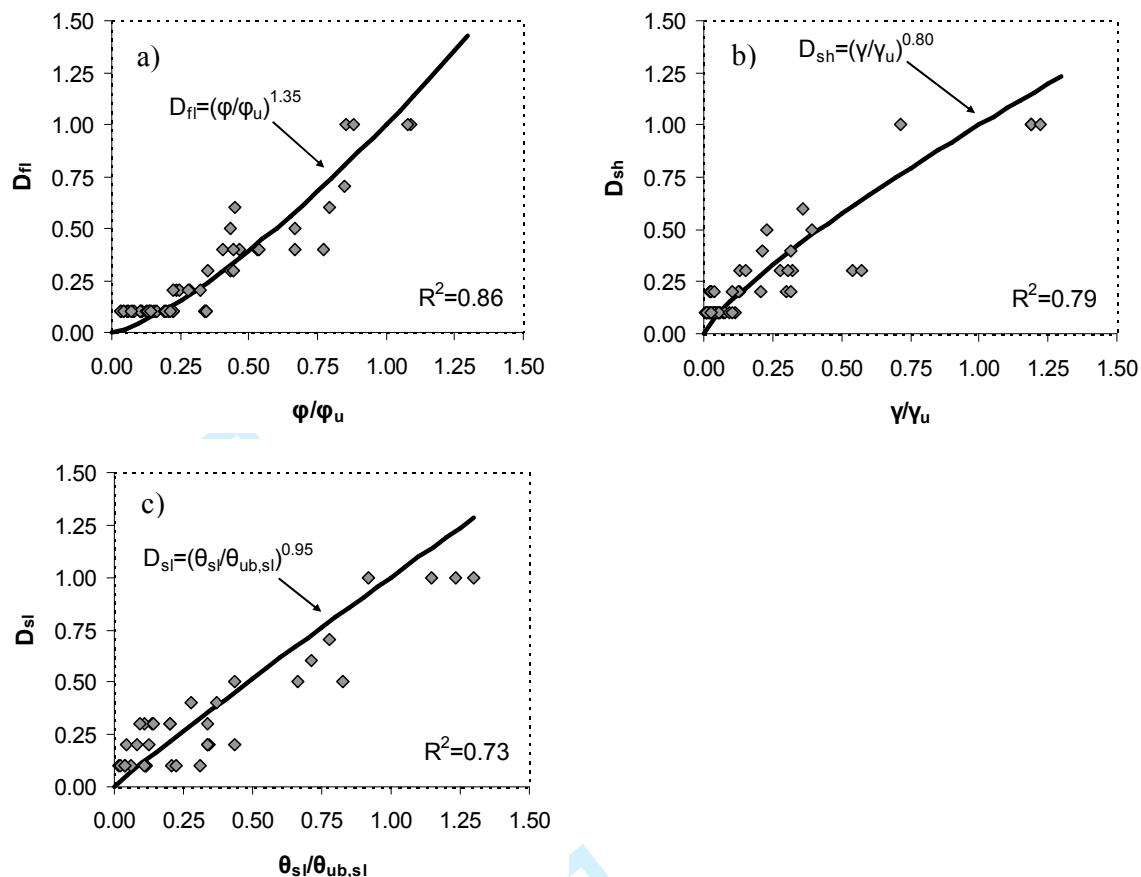
Figure 5: Correlation between the predicted and the experimental individual damage indices: a) flexural index; b) shear index; c) bond index.

In line with the aforementioned observations, Eq. (11) is finally proposed to determine total damage index D_{tot} of the critical end region of an RC member as a function of its individual normalized deformation ratios.

$$D_{tot} = 1 - \left(1 - \left(\frac{\varphi_{\max}}{\varphi_u}\right)^{1.35}\right) \cdot \left(1 - \left(\frac{\gamma_{\max}}{\gamma_u}\right)^{0.80}\right) \cdot \left(1 - \left(\frac{\theta_{sl,\max}}{\theta_{ub,sl}}\right)^{0.95}\right) \tag{11}$$

NUMERICAL MODEL VALIDATION

The member-type finite element model developed by the authors and the local damage index proposed herein were implemented in the computer program IDARC/2D for the nonlinear dynamic analysis of 2D RC structures [32]. To validate the proposed damage model, this program was used to simulate the hysteretic response of several experimental RC columns and frames tested under cyclic or loading, exhibiting different types of failure. It is important to emphasize here that the post-failure range of response is not covered in this study and analysis is terminated at onset of lateral failure.

Based on the analytical results, the proposed seismic damage index is used to describe inelastic damage behaviour of the analysed RC specimens. The predicted

analytical values D_{tot}^{pred} are compared with the observed values D_{tot}^{exp} determined on the basis of the damage scale shown in Table 1. Furthermore, participation of the individual damage mechanisms (flexure, shear, bond), as well as their interaction, to the total damage is investigated. The main findings for each experimental RC specimen (individual member or entire frame) are presented in the following.

Lehman & Moehle column specimen 415

Lehman and Moehle [33] tested five circular RC bridge columns, typical of modern construction, under uniaxial displacement-controlled lateral load reversals in single bending. Herein, the specimen designated as 415 (Fig. 6a) is studied. This specimen was dominated by flexure, exhibiting stable hysteretic behaviour until failure occurred at a ductility $\mu_{\Delta u} \approx 7$. The specimen was subjected to a constant axial load of 654 kN. Concrete strength was 31 MPa and yield strengths of longitudinal and transverse reinforcement were 510 MPa and 607 MPa, respectively.

Fig. (6b) shows the experimental and analytical lateral load vs. total displacement relationship of the specimen. It is seen that the proposed analytical model predicts well the experimental behaviour up to maximum response.

Fig. (6c) shows the development of the individual damage indices D_{fl}, D_{sh} and D_{sl} as a function of the imposed lateral displacement ductility demand, as predicted by the analytical model of this study and as described in the experimental report [33]. In general, very good agreement is observed over the entire range of response.
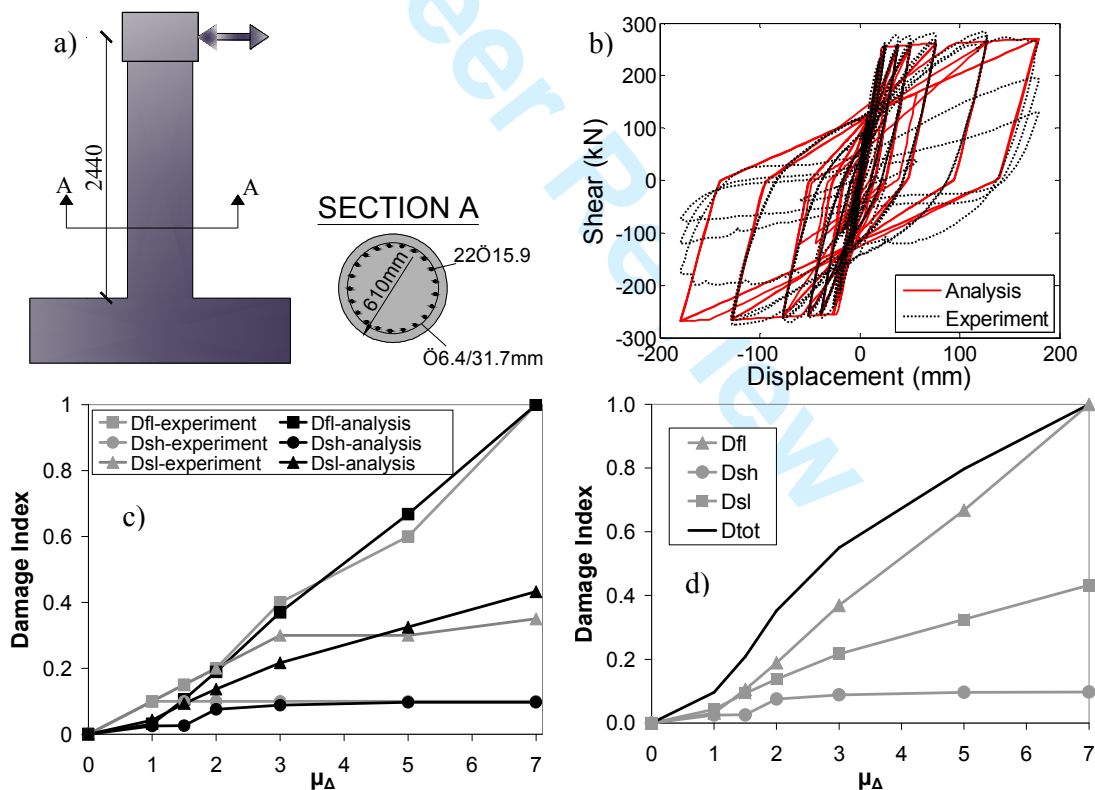

Figure 6: Lehman & Moehle [33] specimen 415: (a) Specimen configuration; (b) Lateral load vs. lateral displacement; (c) Variation of the predicted and experimental individual indices with μ_Δ; (d) Evolution of the analytical damage profile of the RC member.

Finally, Fig. (6d) illustrates the evolution of the damage profile of the examined RC specimen. It can be seen that shear damage remains minor, while bond damage (base cracking) becomes moderate at the end of the analysis. However, flexural damage governs the response of this member and at the end of the analysis D_{fl} becomes equal to unity, indicating a flexural type of failure.

Due to its formulation, the total damage index remains greater than each individual damage index during the entire loading sequence. In this way, combined damage by the individual deformation mechanisms is taken into consideration. At the final step of the analysis, D_{tot} is restrained by D_{fl} and becomes equal to unity as well, revealing the failure damage state of the specimen under examination.

Ranzo & Priestley column specimen HS2

Ranzo & Priestley [34] tested three thin-walled circular hollow columns. Herein, the specimen designated as HS2 is examined, which was designed to fail in shear after yielding in flexure. Specimen configuration is shown in Fig. 7(a). The specimen was subjected to uniaxial displacement-controlled lateral load reversals in single bending under a constant axial load of 1216 kN. Concrete strength was 40 MPa and yield strengths of longitudinal and transverse reinforcement were 450 MPa and 635 MPa, respectively. The column was deemed to have failed at a displacement ductility demand $\mu_{\Delta u} \approx 3.5$ in shear mode after yielding in flexure.
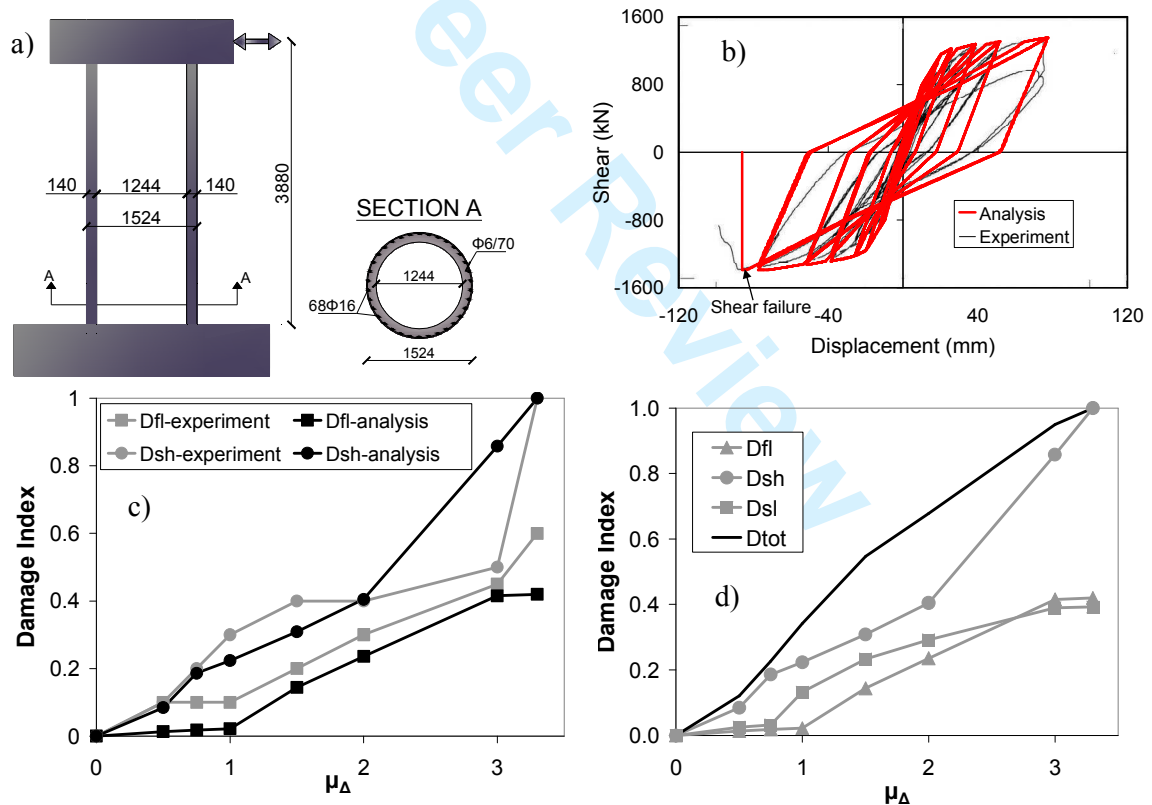

Figure 7: Ranzo & Priestley [34] specimen 415: (a) Specimen configuration; (b) Lateral load vs. lateral displacement; (c) Variation of the predicted and experimental individual indices with μ_Δ; (d) Evolution of the analytical damage profile of the RC member.

Fig. (7b) shows the experimental and analytical lateral load vs. total displacement relationship for the specimen. It can be inferred from the figure that the proposed analytical model captures well the experimental behaviour up to maximum response. Shear failure is predicted at a ductility demand slightly less than 3.5.

Fig. (7c) illustrates the variation of the individual experimental and analytical damage indices D_{fl}, D_{sh}. The D_{sl} index is not included due to lack of sufficient experimental information. It can be observed that flexural damage is captured adequately in the entire range of response. The analytical model follows closely shear damage progression apart from the values corresponding to $\mu_\Delta=3$, where shear damage is overestimated. Nevertheless, shear failure is correctly predicted at $\mu_{\Delta u}\approx3.5$.

Fig. (7d) illustrates the evolution of the damage profile of the examined RC specimen. It can be seen that flexural and bond damage vary from zero to moderate. However, shear damage governs the response of this member and at the end of the analysis D_{sh} becomes equal to unity indicating a shear type of failure. It is important to note that shear damage is predicted by the analytical model due to the application of the shear-flexure interaction procedure described earlier in this study.

Due to its formulation, D_{tot} remains greater than all individual damage indices during the entire loading sequence. In this way, combined damage by the individual deformation mechanisms is taken into consideration. At the final step of the analysis, D_{tot} is restrained by D_{sh} and becomes equal to unity as well, indicating the fact that the specimen begins to lose sharply its lateral force capacity (Fig. 7b).

Melek et al. column specimen S20MI

Melek et al. [15] tested six RC columns with pre-1960's construction details, having lap splice length of 20 bar diameters based on requirements for compression splices in older buildings. Herein, the specimen designated as S20MI is analysed. Specimen configuration is shown in Fig. (8a). It was tested in single bending under cyclic lateral displacements and a 0.20 constant normalized axial load. Concrete strength was 36 MPa and yield strengths of longitudinal and transverse reinforcement were 510 MPa and 480 MPa, respectively. The specimen failed due to bond deterioration in the location of the lap splices prior to yielding in flexure [15].

Fig. (8b) illustrates the experimental and analytical lateral load vs. lateral displacement response. Numerical model is able to capture experimental behaviour adequately up to the onset of lateral strength degradation. Deviation is observed after maximum strength, since the proposed model, at its present state of development, does not address post-peak response. Despite the fact that the analytical model predicts bond failure at 1.6% lateral drift, analysis is carried out up to 2%, where approximately 20% drop in maximum lateral strength was experimentally recorded. This is chosen in order to be able to evaluate the analytical damage index at the experimental failure.

Fig. (8c) illustrates the variation of the individual experimental and analytical damage indices with the imposed lateral drift. It can be observed that both flexural and shear damage are predicted accurately over the entire range of response. Furthermore, the analytical model follows closely bond damage progression. At the end of the analysis (2% drift), bond damage is slightly overestimated (1.23 instead of 1.00). This can be attributed to the simplifying Eq. (5). Nevertheless, it is important to note that the analytical prediction remains on the safe side.

Fig. (8d) illustrates the evolution of the damage profile of the examined RC specimen. It can be seen that flexural damage remains minor (no flexural yielding was recorded), while shear damage becomes moderate during the final steps of the

analysis. However, as recorded experimentally, the prevailing mode of failure is bond damage of the inadequate lap splices. Bond failure ($D_{sl}=1$) is predicted by the analytical model at 1.6% lateral drift. D_{tot} remains slightly greater than D_{sl} over the whole loading sequence and finally becomes equal to unity as well.

   In conclusion, bond damage prevails in the element response. Hence, ignoring this type of damage would drive the analytical procedure to totally erroneous results.
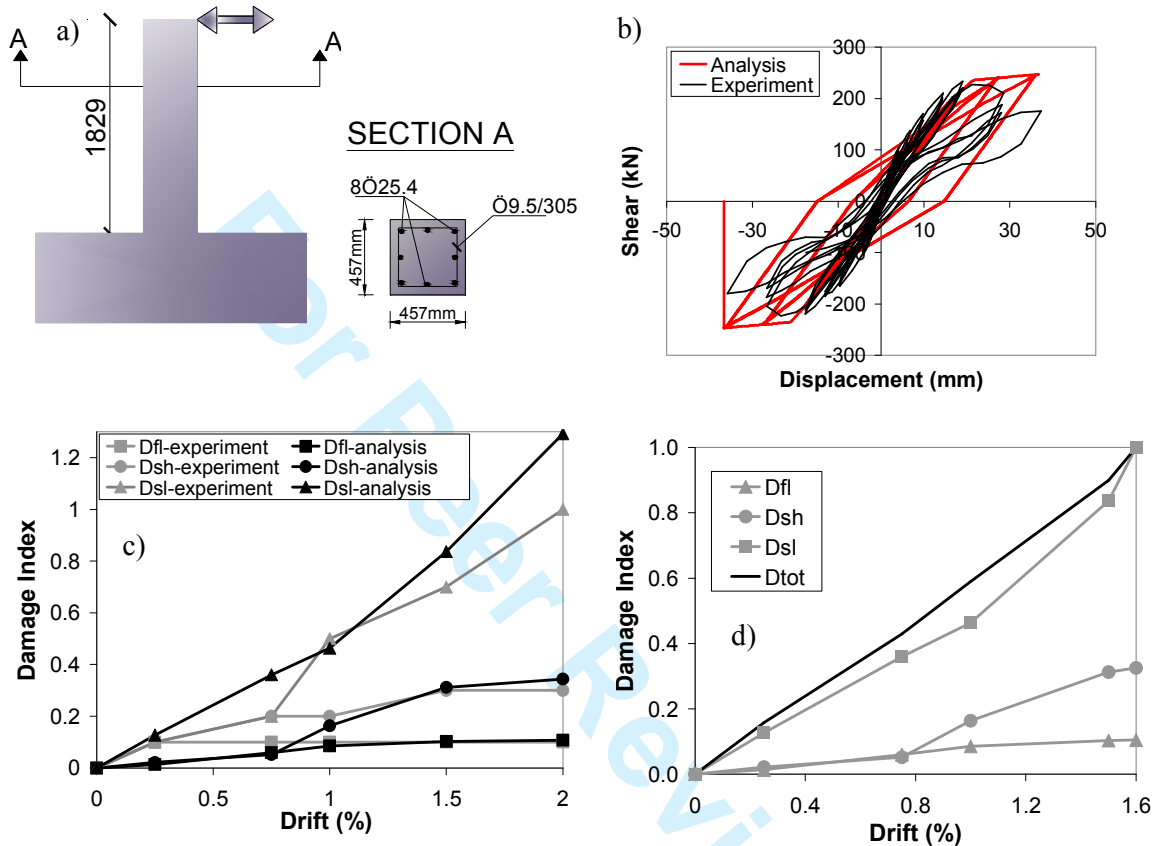

Figure 8: Melek et al. [15] specimen S20MI: (a) Specimen configuration; (b) Lateral load vs. lateral displacement; (c) Variation of the predicted and experimental individual indices with μ_Δ; (d) Evolution of the analytical damage profile of the RC member.

Duong et al. frame specimen

This single-bay, two-storey frame (Fig. 9a) was tested by Duong et al. [35] at University of Toronto. The frame was subjected to a single loading cycle. During the experiment, a lateral load was applied to the second storey beam in a displacement-control mode, while two constant axial loads were applied throughout the testing procedure to simulate the axial load effects of upper stories (Fig. 9a). During loading sequence, the two beams of the frame experienced significant shear damage (close to shear failure) following flexural yielding at their ends [35]. The finite element model applied in this study to predict frame specimen response is also shown in Fig. (9a).
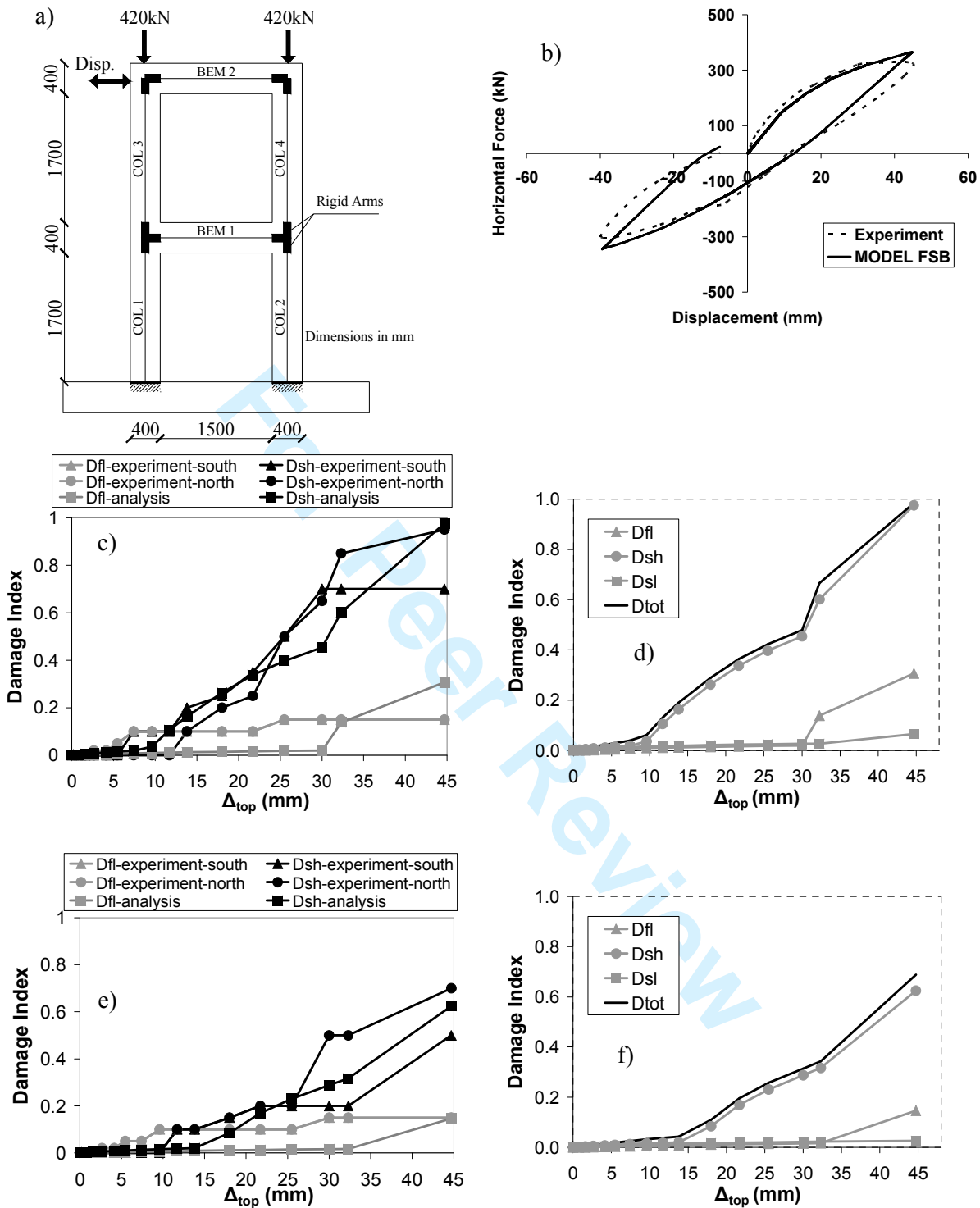
Figure 9: Duong et al. [35] frame specimen: (a) Specimen configuration; (b) Base shear vs. top displacement frame response; (c) Predicted and experimental individual damage indices of the 1st storey beam; (d) Analytical damage indices progression for the 1st storey beam; (e) Predicted and experimental individual damage indices of the 2nd storey beam; (d) Analytical damage indices progression for the 2nd storey beam.

As illustrated in Fig. (9b), the analytical model follows sufficiently close the experimental behaviour over the entire range of response. In addition, the analytical model predicts that both beams develop shear failure after yielding in flexure, as observed in the experimental procedure. Furthermore, it is worth noting that damage to columns of this RC frame was reported to be minor, in close agreement with the analytical prediction.

Figs. (9c)-(9f) present experimental and analytical damage indices progression with the top frame displacement in the positive direction of loading for both RC beam members. At the end of loading in this direction, severe shear cracking was detected in both beam elements. Especially for the 1st storey beam, a 9 mm wide shear crack formed, indicating imminent shear failure.

Figs (9c) and (9e) present the comparison of the predicted and the experimental individual flexural and shear damage indices for the 1st and 2nd storey beam respectively. Despite the symmetrical configuration of the RC frame, shear damage was found in the test to differ between the north and south beam ends. Hence, experimental damage propagation for both beam ends is presented.

The analytical model predicts the same structural damage for both beam ends and the predicted damage indices reasonably match their experimental counterparts. Flexural damage is slightly underestimated in the first stages of loading, but is predicted well at the end of the analysis. Shear damage is predicted to be major-to-severe for both beam members. Especially for the 1st storey beam, D_{sh} is predicted to be very close to unity (0.97) indicating shear failure in accordance with the experimental observations.

Figs (9d) and (9f) illustrate the development of the predicted damage profiles with the imposed lateral top displacement for the 1st and 2nd storey beams, respectively. It can be seen that shear damage almost completely governs the response and D_{tot} is only marginally greater than D_{sh} for both members. At the end of the analysis, D_{tot} becomes 0.98 for the 1st storey beam, indicating imminent failure of this member.

CONCLUSIONS

A new combined local damage index for existing RC members was introduced, which treats degradation caused by all deformation mechanisms (flexure, shear, bond-slip) in an explicit and discrete manner. The index is capable of capturing the additive character of deterioration coming from the three inelastic response mechanisms, as well as the increase in damage caused by their interaction.

Initially, the proposed damage index is calibrated against experimental data involving damage evolution in 12 RC column specimens. To this cause, a new damage scale with three distinct damage levels for each deformation mechanism is introduced. Based on this damage scale and the experimental observations, the parameters of the proposed index are calibrated. Sufficient correlation is achieved with the experimental evidence. However, the need of further calibrating the damage index with experimental data is emphasized.

Next, the local damage index is applied in conjunction with a finite element model developed by the authors to predict the damage state of several test specimens, including both individual RC columns and an entire frame with substandard detailing. It is concluded that in all cases and irrespective of the prevailing mode of failure, the new local damage index describes well the damage state of the analysed specimens up to the onset of failure. Further research is required towards modelling structural response and quantifying structural damage in the post peak range of response.

REFERENCES

1. Pincheira J, Dotiwala F, Souza J. Seismic analysis of older reinforced concrete columns. *Earthquake Spectra* 1999; **15**: 245-272.

2. Consenza E, Manfredi G, Verderame GM. Seismic assessment of gravity load designed RC frames: Critical issues in structural modelling. *Journal of Earthquake Engineering* 2002; **6** (1): 101-122.

3. Elwood K, Moehle J. Dynamic collapse analysis for a reinforced concrete frame sustaining shear and axial failures. *Earthquake Engineering and Structural Dynamics* 2008; **37** (7): 991-1012.

4. Sezen H, Chowdhury T. Hysteretic model for reinforced concrete columns including the effects of shear and axial load failure. *Journal of Structural Engineering (ASCE)* 2009; **135** (2): 139-146.

5. Mergos PE, Kappos AJ. A distributed shear and flexural flexibility model with shear-flexure interaction for RC members subjected to seismic loading. *Earthquake Engineering and Structural Dynamics* 2008; **37** (12): 1349-1370.

6. Mergos PE, Kappos AJ. A gradual spread inelasticity model for R/C beam-columns, accounting for flexure, shear and anchorage slip. *Engineering Structures* 2012; **44**: 94-106.

7. Mergos PE. Assessment of seismic behaviour of existing RC structures. *PhD Thesis*. Aristotle University of Thessaloniki, Greece, 2010.

8. Mergos PE, Kappos AJ. Seismic damage analysis of RC structures with substandard detailing. *Proc. of the 3ʳᵈ COMPDYN Conference*, Corfu, Greece, 2011, paper no. 304.

9. Kappos AJ. Seismic damage indices for RC buildings: evaluation of concepts and procedures. *Progress in Structural Engineering and Materials* 1997; **1** (1): 78-87.

10. Cosenza E, Manfredi G. Damage indices and damage measures. *Progress in Structural Engineering and Materials* 2000; **2** (1): 50-59.

11. Park YJ, Ang AHS. Mechanistic seismic damage model for reinforced concrete. *Journal of Structural Engineering (ASCE)* 1985; **111** (4): 722–739.

12. Williams M, Villemure I, Sexsmith R. Evaluation of seismic damage indices for concrete elements loaded in combined shear and flexure. *ACI Structural Journal* 1997; **94** (3): 315-322.

13. Mergos PE, Kappos AJ. Seismic damage analysis including inelastic shear-flexure interaction. *Bulletin of Earthquake Engineering* 2010; **8** (1): 27-46.

14. Pantelides CP, Hansen J, Nadauld J, Reaveley LD. *Assessment of reinforced concrete building exterior joints with substandard details*. PEER Report 2002/18, Univ. California, Berkeley, 2002.

15. Melek M, Wallace JW, Conte JP. *Experimental assessment of columns with short lap splices subjected to cyclic loads*. PEER Report 2003/04, Univ. California, Berkeley, 2004.

16. Mander JB, Priestley MJN, Park R. Theoretical stress-strain model for confined concrete. *Journal of Structural Engineering* 1986; **114** (8): 1804-1825.

17. Papia M, Russo G. Compressive concrete strain at buckling of the longitudinal reinforcement. *Journal of Structural Engineering* 1989; **115** (2): 382-397.

18. Sivaselvan MV, Reinhorn, AM. Hysteretic models for deteriorating inelastic structures. *Journal of Engineering Mechanics* 2000; **126** (6): 633-640.

19. Soleimani D, Popov EP, Bertero VV. Nonlinear beam model for RC frame analysis. *Proc. of Seventh Conference on Electronic Computation*, St. Louis, Misouri, 1979.

20. Ozcebe G, Saatcioglu M. Hysteretic shear model for reinforced concrete members. *Journal of Structural Engineering* 1989; **115** (1): 132-148.

21. Park R, Paulay T. *Reinforced concrete structures.* Wiley: New York, 1975.

22. Priestley MJN, Verma R, Xiao Y. Seismic shear strength of reinforced concrete columns. *Journal of Structural Engineering (ASCE)* 1994; **120** (8): 2310-2329.

23. Alsiwat JM, Saatcioglu M. Reinforcement anchorage slip under monotonic loading. *Journal of Structural Engineering* 1992; **118** (9): 2421-2438.

24. ACI Committee 408. *Bond and development of straight reinforcement in tension.* American Concrete Institute: Farmington Hills, 2003.

25. CEB Bulletin No. 213/214. *CEB-FIP model code 90.* Lausanne, 1993.

26. Saatcioglu M, Alsiwat J., Ozcebe G. Hysteretic behaviour of anchorage slip in RC members. *Journal of Structural Engineering (ASCE)* 1992; **118** (9): 2439-2458.

27. Cho JJ, Pincheira JA. Inelastic analysis of RC columns with short lap splices subjected to reversed cyclic loading. *ACI Structural Journal* 2006; **103** (2): 280-290.

28. Kappos AJ, Xenos A. A reassessment of ductility and energy-based seismic damage indices for reinforced concrete structures. *Proc. of Eurodyn, Balkema, Rotterdam*, 1996.

29. Mehanny SSF, Deierlein GGD. Seismic damage and collapse assessment of composite moment frames. *Journal of Structural Engineering (ASCE)* 2001; **127** (9): 1045-1053.

30. FEMA-356. *Prestandard and commentary for the seismic rehabilitation of buildings.* Federal Emergency Management Agency, Washington, 2000.

31. EEPO. *Guidelines for pre-earthquake and post-earthquake interventions to buildings.* Earthquake Planning and Protection Organization, Ministry of Public Works, Athens, Greece, 2001.

32. Valles RE, Reinhorn AM, Kunnath SK, Li C, Madan A. *IDARC2D Version 4.0: A program for the inelastic damage analysis of buildings.* Technical Report NCEER-96-0010, State University of New York at Buffalo, New York, 1996.

33. Lehman D, Moehle JP. *Seismic performance of well confined concrete bridge columns.* PEER Report 1998/01, Univ. of California, Berkeley, 1998.

34. Ranzo G, Priestley MJN. *Seismic performance of circular hollow columns subjected to high shear.* Report No. SSRP-2001/01, University of San Diego, California, 2001.

35. Duong KV, Sheikh FJ, Vecchio F. Seismic behaviour of shear critical reinforced concrete frame: Experimental Investigation. *ACI Structural Journal 2007*; **104**(3): 304-313.